Photodegradation of Methylene Blue Using Crystalline Titanosilicate Quantum-Confined Semiconductor

Vittorio Luca,*,† Michael Osborne,† Devlet Sizgek,† Christopher Griffith,† and Paula Z. Araujo‡

Australian Nuclear Science and Technology Organisation, Institute of Materials and Engineering Sciences, PMB 1, Menai, 2234, Australia, and Unidad de Actividad Química, Centro Atómico Constituyentes, Comisión Nacional de Energía Atómica, Avenida General Paz 1499,1650 San Martín, Provincia de Buenos Aires, Argentina

Received December 23, 2005. Revised Manuscript Received September 20, 2006

Synthetic sitinakite contains in its structure a discrete wire-like sublattice of linked TiO_6 octahedra. This sublattice is held apart by silicate tetrahedra forming one-dimensional channels that run down the *c* axis. The optical properties of this structural arrangement have been studied and compared with other titanosilicate phases, the best known being ETS-10. Thus, sitinakite which has twice the titanate wire diameter of ETS-10 has a band gap of 4.07 eV compared with 3.87 eV. The reduced electron−hole effective mass of the sitinakite quantum-confined system has been calculated through use of the effective mass model and compared with that of other titanosilicate materials. The sitinakite phase has been shown to effectively photodegrade methylene blue (MB) dye at pH 7 using visible light excitation and displays a higher degradation rate than TiO_2 (Degussa, P25) under the same experimental conditions. On the contrary, under UV excitation, the photodegradation rate obtained using P25 is much higher than that using sitinakite. Given that the band edge of sitinkaite is significantly blue shifted compared with that of P25, photodegradation of MB using sitinakite is attributed to sensitization of the MB cationic dye which is strongly adsorbed onto the negatively charged sitinakite surfaces.

Introduction

Mounting environmental concerns have made titania photocatalysis an extensively researched subject. Numerous reviews are available on materials properties and mechanisms and the reactions that can be carried out with this material.[1−4] Titania is the most successful semiconductor for water splitting and photodegradation of organic pollutants. However, it has a wide band gap of 3.2 eV which results in utilization of about only 3% of the solar spectrum. This in turn makes it photochemically more stable than any other photocatalyst.

Dye pollutants that absorb visible light are produced by the textile and photographic industries, and their influence on the environment is of increasing concern. Consequently, there are now many reports of photomineralization of such dyes using titania-based catalysts.[5−17] However, the mechanism of photodegradation can be different depending on whether illumination is with UV or visible light, the latter being favored. If visible light is used, then the dye itself can be photoexcited (sensitized) and electron transfer may then occur from the excited dye molecule into the conduction band of the semiconductor. For UV excitation the reverse is usually the case.[6]

Recently, the photocatalytic decomposition of acetaldehyde has been studied using the titanosilicate cation exchanger, ETS-10, under UV and visible light illumination. In its Na/K-exchanged form, ETS-10 shows significant activity under UV illumination, and this could be enhanced by incorporation of extra framework or exchangeable cations such as Co or Ag present within the channel system. Neither titania or as-prepared ETS-10 showed activity on illumination with visible light, but the metal-loaded and heated ETS-10 samples did

* To whom correspondence should be addressed. Phone: 61-2-9717 3087. Fax: 61-2-9543 7179. E-mail: vlu@ansto.gov.au.
† Australian Nuclear Science and Technology Organisation.
‡ Unidad de Actividad Química.

(1) Anpo, M.; Takeuchi, M. *J. Catal.* **2003**, *216*, 505.
(2) Anpo, M. *Pure Appl. Chem.* **2000**, *72*, 1265.
(3) Beydoun, D.; Amal, R.; Low, G.; McEvoy, S. *J. Nanoparticle Res.* **1999**, *1*, 439.
(4) Hoffmann, M. R.; Martin, S. T.; Choi, W. Y.; Bahnemann, D. W. *Chem. Rev.* **1995**, *95*, 69.
(5) Wahi, R. K.; Yu, W. W.; Liu, Y. P.; Mejia, M. L.; Falkner, J. C.; Nolte, W.; Colvin, V. L. *J. Mol. Catal. A: Chem.* **2005**, *242*, 48.
(6) Liu, G.; Wu, T.; Zhao, J.; Ohidaka, H.; Serpone, N. *Environ. Sci. Technol.* **1999**, *33*, 2081.
(7) Epling, G. A.; Lin, C. *Chemosphere* **2002**, *46*, 561.
(8) Banat, F.; Al-Asheh, S.; Al-Rawashdeh, M.; Nusair, M. *Desalination* **2005**, *181*, 225.
(9) Fetterolf, M. L.; Patel, H. V.; Jennings, J. M. *J. Chem. Eng. Data* **2003**, *48*, 831.
(10) Senthilkumaar, S.; Porkodi, K.; Gomathi, R.; Maheswari, A. G.; Manonmani, N. *Dyes Pigm.* **2006**, *69* (1−2), 22−30.
(11) Prieto, O.; Fermoso, J.; Nunez, Y.; Del Valle, J. L.; Irusta, R. *Sol. Energy* **2005**, *79*, 376.
(12) Liu, C. C.; Hsieh, Y. H.; Lai, P. F.; Li, C. H.; Kao, C. L. *Dyes Pigm.* **2006**, *68*, 191.
(13) Akbal, F. *Environ. Prog.* **2005**, *24*, 317.
(14) Toor, A. P.; Verma, A.; Jotshi, C. K.; Bajpai, P. K.; Singh, V. *Dyes Pigm.* **2006**, *68*, 53.
(15) Mahmoodi, N. M.; Arami, M.; Limaee, N. Y.; Tabrizi, N. S. *Chem. Eng. J.* **2005**, *112*, 191.
(16) Muruganandham, M.; Swaminathan, M. *Dyes Pigm.* **2006**, *68* (2−3), 133−142.
(17) Zainal, Z.; Hui, L. K.; Hussein, M. Z.; Taufiq-Yap, Y. H.; Abdullah, A. H.; Ramli, I. *J. Hazard. Mater.* **2005**, *125*, 113.

10.1021/cm052839p CCC: $33.50
Published on Web 12/19/2006

show some activity.[18] It is indeed interesting that a material such as this can function as a catalyst at all given its structural and electronic characteristics, which will be described later. Use of titanosilicate materials such as ETS-10 therefore deserves and is receiving greater consideration, especially in the context of the degradation of dye and other pollutant molecules. The influence of the ion-exchange form of the material has been investigated.[19,20] While other studies have highlighted the potential for shape-selective photocatalysis by these materials.[21−23] ETS-10 materials have also recently shown activity for the photocatalytic production of hydrogen from water when small semiconductor particles are incorporated.[24]

Crystalline titanosilicates represent a small but much studied class of microporous materials with mixed metal coordination, meaning that SiO_4 tetrahedra and TiO_6 octahedra share corners and edges to form a microporous zeolite-like network of channels. A well-known example of this material is the previously mentioned ETS-10 (Engelhard TitanoSilicate number 10), and this material has been investigated extensively because of its unusual structural[25−30] and ion-exchange properties. The structure of ETS-10 comprises linear arrays of linked TiO_6 octahedra resembling a wire (Figure 1c). These titanate wires are in turn linked by silicate units to form a complex array in which the wire-like arrangement is maintained. The absorption spectrum of ETS-10 has been reported and the optical gap determined to be 3.8 eV. This represents a significant blue shift from that of bulk titania (3.2 eV).[31] This wire-like arrangement has been the subject of further investigation, and it has been concluded that quantum confinement, which remains under dispute in TiO_2,[32] occurs in the wires of ETS-10.[33,34]

While ETS-10 is perhaps the best studied titanosilicate, other members of the titanosilicate family have recently started to receive attention including penkvilksite,[35−37] nenadkevichite,[38,39] and sitinakite.[40−43] Like ETS-10, the sitinakite phase has a structure in which titanium and silicon atoms are also present in 6- and 4-fold coordination, respectively. The structure of sitinakite and its variants has been amply studied and is now fully described.[41,44−47] It consists of titanium octahedra that are linked in a cubane-like arrangement to form chains or wires that are held apart by silicate tetrahedra to form a network of unidimensional channels that run down the *c*-crystallographic axis (Figure 1a). The dimension of these channels is only on the order of a few angstroms. Compared to ETS-10, this channel network is far simpler. Like ETS-10, exchangeable cations are accommodated within these channels and compensate charge on the framework. Sitinakite therefore has a structure that is similar to that of the related titanosilicates ETS-10. The unusual channel architecture of ETS-10 is one reason why it has been extensively studied. When the silicate units are stripped away (Figure 1b) it is apparent the quantum wires in sitinakite are approximately twice the diameter of those

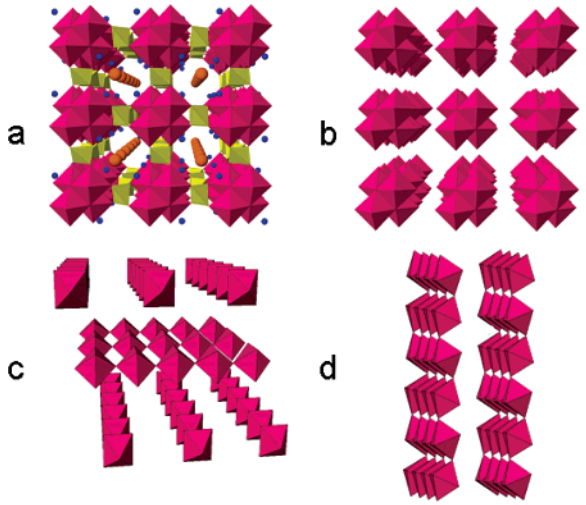

Figure 1. Polyhedral representation of (a) sitinakite and titanate sublattices of titanosilicates after removal of the silicate tetrahedra for (b) sitinakite, (c) ETS-10, and (d) nenadkevichite.

(18) Uma, S.; Rodrigues, S.; Martyanov, I. N.; Klabunde, K. J. *Microporous Mesoporous Mater.* **2004**, *67*, 181−187.
(19) Krisnandi, Y. K.; Howe, R. F. *Appl. Catal. A* **2006**, *307* (1), 62−69.
(20) Howe, R. F.; Krisnandi, Y. K. *Chem. Commun.* **2001**, 1588−1589.
(21) Xamena, F. X. L. I.; Calza, P.; Lamberti, C.; Prestipino, C.; Damin, A.; Bordiga, S.; Pelizzetti, E.; Zecchina, A. *J. Am. Chem. Soc.* **2003**, *125*, 2264.
(22) Calza, P.; Paze, C.; Pelizzetti, E.; Zecchina, A. *Chem. Commun.* **2001**, 2130.
(23) Usseglio, S.; Calza, P.; Damin, A.; Minero, C.; Bordiga, S.; Lamberti, C.; Pelizzetti, E.; Zecchina, A. *Chem. Mater.* **2006**, *18*, 3412.
(24) Guan, G. Q.; Kida, T.; Kusakabe, K.; Kimura, K.; Abe, E.; Yoshida, A. *Appl. Catal. A* **2005**, *295*, 71.
(25) Anderson, M. W.; Agger, J. R.; Luigi, D. P.; Baggaley, A. K.; Rocha, J. *Phys. Chem. Chem. Phys.* **1999**, *1*, 2287.
(26) Anderson, M. W.; Philippou, A.; Lin, Z.; Ferreira, A.; Rocha, J. *Angew. Chem., Int. Ed. Engl.* **1995**, *34*, 1003.
(27) Anderson, M. W.; Rocha, J.; Lin, Z.; Philippou, A.; Orion, I.; Ferreira, A. *Microporous Mater* **1996**, *6*, 195.
(28) Anderson, M. W.; Terasaki, O.; Ohsuna, T.; Malley, P. J. O.; Philippou, A.; MacKay, S. P.; Ferreira, A.; Rocha, J.; Lidin, S. *Philos. Mag. B* **1995**, *71*, 813.
(29) Anderson, M. W.; Terasaki, O.; Ohsuna, T.; Philippou, A.; MacKay, S. P.; Ferreira, A.; Rocha, J.; Lidin, S. *Nature* **1994**, *367*, 347.
(30) Anderson, M. W.; Terasaki, O.; Ohsuna, T.; Philippou, A.; MacKay, S. P.; Ferreira, A.; Rocha, J.; Lidin, S. *Stud. Surf. Sci. Catal.* **1995**, *98*, 258.
(31) Borello, E.; Lamberti, C.; Bordiga, S.; Zecchina, A.; Arean, C. O. *Appl. Phys. Lett.* **1997**, *71*, 2319.
(32) Monticone, S.; Tufeu, R.; Kanaev, A. V.; Scolan, E.; Sanchez, C. *Appl. Surf. Sci.* **2000**, *162*, 565−570.
(33) Bordiga, S.; Palomino, G. T.; Zecchina, A.; Ranghino, G.; Giamello, E.; Lamberti, C. *J. Chem. Phys.* **2000**, *112*, 3859.
(34) Damin, A.; Llabres i Xamena, F. X.; Lamberti, C.; Civalleri, B.; Zicovich-Wilson, C. M.; Zecchina, A. *J. Phys. Chem. B* **2004**, *108*, 1328.
(35) Lin, Z.; Rocha, J.; Brandao, P.; Ferreira, A.; Esculcas, A. P.; Dejesus, J. D. P.; Philippou, A.; Anderson, M. W. *J. Phys. Chem. B* **1997**, *101*, 7114.
(36) Liu, Y. L.; Du, H. B.; Xu, Y. H.; Ding, H.; Pang, W. Q.; Yue, Y. *Microporous Mesoporous Mater* **1999**, *28*, 511.
(37) Liu, Y.; Du, H.; Zhou, F.; Pang, W. *Chem. Commun.* **1997**, 1467.
(38) Cruciani, G.; Deluca, P.; Nastro, A.; Pattison, P. *Microporous Mesoporous Mater.* **1998**, *21*, 143.
(39) Rocha, J.; Brandao, P.; Lin, Z.; Kharlamov, A.; Anderson, M. W. *Chem. Commun.* **1996**, 669.
(40) Tripathi, A.; Medvedev, D. G.; Clearfield, A. *J. Solid State Chem.* **2005**, *178*, 253.
(41) Luca, V.; Hanna, J. V.; Smith, M. E.; James, M.; Mitchell, D. R. G.; Bartlett, J. R. *Microporous Mesoporous Mater* **2002**, *55*, 1.
(42) Kostov-Kytin, V.; Mihailova, B.; Kalvachev, Y.; Tarassov, M. *Microporous Mesoporous Mater.* **2005**, *86*, 223.
(43) Medvedev, D. G.; Tripathi, A.; Clearfield, A.; Celestian, A. J.; Parise, J. B.; Hanson, J. *Chem. Mater.* **2004**, *16*, 3659.
(44) Poojary, D. M.; Bortun, A. I.; Bortun, L. N.; Clearfield, A. *Inorg. Chem.* **1996**, *35*, 6131.
(45) Poojary, D. M.; Cahill, R. A.; Clearfield, A. *Chem. Mater.* **1994**, *6*, 2364.
(46) Larentzos, J. P.; Clearfield, A.; Tripathi, A.; Maginn, E. J. *J. Phys. Chem. B* **2004**, *108*, 17560.
(47) Tripathi, A.; Medvedev, D. G.; Delgado, J.; Clearfield, A. *J. Solid State Chem.* **2004**, *177*, 2903.

in ETS-10, and this raises the prospect of interesting electronic properties and, in turn, applications. For instance, the redox activity of the titanate sublattice and structural stability give this material a high capacity for Li insertion.[48]

The synthetic analogue of the sitinakite mineral phase was initially developed by DOE researchers for treatment of radioactive waste, has exceptional selectivity for $^{137}Cs^{+}$ and $^{90}Sr^{2+}$ in alkaline media, and has been much studied in this context.[49−51] Its ion-exchange properties and structural properties have also been investigated. However, beyond our attempts to deploy these materials in battery electrodes,[48] few other applications have so far been explored for this extremely interesting material. Nor have quantum confinement effects received any attention.

The aim of this paper is 2-fold. First, to shed light on quantum confinement effects in sitinakite in comparison with other similarly structured materials, and second, to investigate the photomineralization of a cationic dye using sitinakite in comparison with P25 using both visible and UV light excitation.

Experimental Section

TiO_2 was obtained from a commercial source (Degussa P25, Anatase:Rutile ratio of approximately 80:20). Sitinikite variants were synthesized in the laboratory according to previously published proceedures.[41,44] The surface areas of these two materials are 50 and 47 m^2/g for P25 and sitinakite, respectively. A high surface area implies a larger area for chemisorption and therefore a larger surface over which the catalyzed reaction can take place. Hence, surface area could be expected to have a significant effect on photocatalytic decay rate. However, given the similar surface areas of both Sitinikite and Degussa P25, this should not be a factor in our work.

All solutions were prepared from Millipore water, and methylene blue was used as received. The solution pH was altered where required by adding small volumes of 0.10 mol/L HCl and 0.10 mol/L NaOH. As noted by Bhatkhande,[52] chloride ions can inhibit the adsorption of MB onto our catalysts. However, the concentrations of chloride ions due to the small amounts of acid added for pH adjustment are far lower than that shown to affect adsorption. Hence, for all practical purposes this effect can be regarded as negligible.

Photocatalytic reactions took place in a jacketed glass flask (Figure 2). Prior to switching on the light source a strong flow of air was bubbled through the solution via a top-mounted air diffuser tube. This should ensure that MB is in its oxidized state and eliminate the confusion between the desired true mineralization of MB and production of colorless Leuco-MB, as the excess oxygen acts to oxidize the Leuco-MB back to MB.[53] Air flow rate during irradiation was found to have a noticeable effect on reaction rate due to its mixing effects and modification of the optical properties

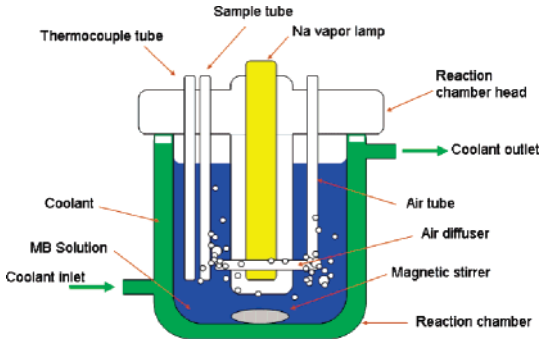

Figure 2. Schematic of reactor used for the visible light photodecomposition of MB.

of the air/water mixture. Hence, air flow rate was kept constant at roughly 300 mL/min throughout experiments. Other tubes were inserted into solution for temperature measurement and sampling.

The head of the reaction chamber was designed to accommodate a Na-vapor lamp being inserted into the center of the chamber. The total capacity of the chamber with head in place was approximately 700 mL. In the case of visible light irradiation, the lamp used was a Sylvania SHPT-GRO 400 Na-vapor lamp, which relatively closely matches the solar spectrum. The experiment was draped in black cloth to eliminate any unwanted environmental irradiation. This lamp generated a significant amount of heat, and so the operating voltage was limited to 180 V by a variac to reduce heat output. Chamber temperature was found to have a significant influence on reaction rate, necessitating the use of a cooling system to keep temperature stable. Coolant was pumped from the chiller into the reaction chamber jacket and then into a fan-cooled radiator. A temperature of 40 ± 2 °C was maintained throughout our experiments.

In the case of UV light irradiation, the lamp used was a UV source (a 15 W UV lamp with a maximum wavelength of 365 nm). A cooling system was also employed, and the temperature was maintained at around 20 ± 2 °C. The experiment was draped in black cloth to eliminate any unwanted environmental irradiation. The light intensity on the irradiated surface area was 7.651020 photons/s as measured by potassium ferrioxalate actinometry.

Catalysts were suspended in the MB solutions at typical catalyst concentrations of 0.522 g/L and constantly stirred magnetically. MB degradation was followed spectrophotometrically monitoring the absorbance at 674 nm using a Perkin-Elmer Lambda 40 UV−vis spectrometer. It is to be noted that the spectrum changed slightly with the progress of the photocatalytic reaction with the primary peak undergoing a slight blue shift on the order of a couple of nanometers after 2 h of reaction time. After pH alteration was complete, the solution was left covered for an hour to reach its adsorption/desorption equilibrium condition. Thirty min was allowed after activation of the lamp for the lamp to warm up and for thermal equilibrium to be reached. Subsequent to this, 4 mL samples were taken every 10 min until 12 samples had been taken. Samples were syringed from the reaction chamber via sampling tube and then their pH measured. Samples were then passed through a 0.45 μm filter in order to remove all catalyst and stored in a sealed box before being analyzed in the spectrometer.

X-ray absorption near edge (XANES) spectra were recorded at the Ti K edge in 0.10 eV steps in transmission mode on a beamline 20B at the Photon Factory, Tsukuba, Japan, using a Si(111) double monochromator. An estimate of the resolution ($\Delta E/E$) was calculated from the Darwin width of the Si(111) monochromator and the slit opening of 0.4 mm, and a value of 1.36 eV was obtained. This value was very similar to the peak-to-peak first-derivative line width obtained for a Ti foil reference spectrum. Samples were

(48) Milne, N. A.; Griffith, C. S.; Hanna, J. V.; Skyllas-Kazacos, M.; Luca, V. *Chem. Mater.* **2006**, *18*, 3192.
(49) Anthony, R. G.; Philip, C. V.; Dosch, R. G. *Waste Manage.* **1993**, *13*, 503.
(50) Anthony, R. G.; Dosch, R. G.; Gu, D.; Philip, C. V. *Ind. Eng. Chem. Res.* **1994**, *33*, 2702.
(51) Gu, D.; Nguyen, L.; Philip, C. V.; Huckman, M. E.; Anthony, R. G.; Miller, J. E.; Trudell, D. E. *Ind. Eng. Chem. Res.* **1997**, *36*, 5377.
(52) Bhatkhande, D.; Pangarkar, V. G.; Beenackers, A. A. C. M. *J. Chem. Technol. Biotechnol.* **2001**, *77*, 102.
(53) Mills, A.; Wang, J. S. *J. Photochem. Photobiol. A* **1999**, *127* (1−3), 123−134.

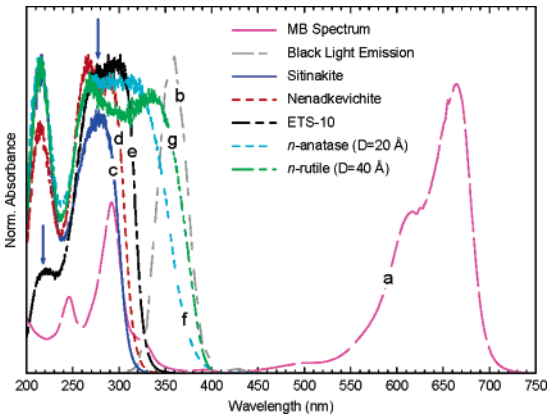

Figure 3. UV−vis spectrum of sitinakite in comparison to other titanosilicates and titanates: (a) MB, (b) black light emission, (c) sitinakite, (d) nenadkevichite, (e) ETS-10, (f) nanocrystalline anatase, $D = 20$ Å, and (g) nanocrystalline rutile, $D = 40$ Å. D is the average particle diameter.

diluted by mixing boron nitride and then loaded into sample holders with Kapton windows.

Zeta potential measurements were performed on a Malvern Zetasizer 2000.

Results and Discussion

Electronic Properties of Titanosilicates. In Figure 1 are shown polyhedral representations of the titanate sublattice chains observed in the three different titanosilicate materials of interest. ETS-10 and nenadkevichite possess single chains with different configurations, while sitinakite possesses double chains. The effective mass model (EMM) provides the band-gap shift of a quantum-confined semiconductor with respect to that of the corresponding bulk semiconductor.[54,55] Lamberti[56] recently showed that the band gap of the titanate sublattice in a commercial ETS-10 sample was significantly blue shifted relative to that of bulk titanates such as anatase and rutile. They were further able to determine the reduced effective reduced mass, μ, of electrons and holes in this one-dimensional quantum wire using the EMM as follows

$$\Delta E_g = \frac{h^2}{4\mu_{xy}d^2} + \frac{h^2}{8\mu_z L^2} \approx \frac{h^2}{4\mu_{xy}d^2}$$

This equation applies to a quantum-confined wire with a diameter d and length L.

Optical (diffuse reflectance) spectra of the three different titanosilicates are shown in Figure 3. A large difference in absorption edge onset is observed between the anatase and rutile nanoparticles and the titanosilicate materials. The absorption onset for P25 occurs around 400 nm[57] as for the rutile sample investigated here. The values of E_g determined for the three titanosilicate systems were 3.87, 3.99, and 4.07 eV for ETS-10, nenadkevikite, and sitinakite respectively (assuming direct band gap). The value of 3.87 eV for ETS-10 is somewhat lower than the value of 4.03 eV determined by Borello[31] for their ETS-10 sample. Such a discrepancy may be explained by the fact that the sample investigated by these researchers was a commercial sample with probably lower crystallinity.[58]

In the case of the titanosilicate materials examined here it is valid to assume that L is close to being equal to the average crystallite diameters which is in the micrometer range (see Figures 4 and 5). This assumption might be expected to hold in the absence of significant wire disruptions due to defects. For the materials under investigation here L is large with respect to d, and therefore, the second term in the above expression can be dropped. However, μ, being a property of the band structure, will vary depending on the material. Application of the EMM therefore affords a method of estimating μ for each of the titanosilicate materials in a similar manner to that done for ETS-10 by Lamberti et al.[56] Taking ΔE_g as the difference between the band gap calculated from the data of Figure 3 and the value for bulk anatase ($E_g = 3.20$ eV) we arrive at values for μ of $2.51m_e$, $2.12m_e$, and $0.54m_e$ (where m_e is the electron rest mass) for ETS-10, nenadkevichite, and sitinakite respectively. The value for the reduced effective mass of the ETS-10 prepared here is somewhat larger than the value of $1.97m_e$ determined by Lamberti et al. for a commercial ETS-10 sample. Since the commercial ETS-10 sample has the same value of d as our sample, it is difficult to know to what to ascribe the disparity in μ values. Here we note that L in the poorly crystalline commercial sample is lower than in the ETS-10 sample prepared here (see X-ray diffraction pattern in Supporting Information) due to the fact that the wires in the former are interrupted by defects.[58] Taking this one step further in Figure 6 we plot E_g and μ values as a function of crystallite diameter (Figure 5) and note that there is a relatively clear trend. While it is not impossible that the trend is entirely fortuitous given the small number of data points, it might also point to deficiencies in the EMM. Such deficiencies have been highlighted previously.[59]

A qualitative indication of the density of states in these quantum-confined sublattice systems can be gauged from pre-edge features in the X-ray absorption near-edge structure (XANES) which is essentially a map of the density of states.[60] For the nanocrystalline anatase and rutile materials (Figure 7a,b) three well-developed transitions are observed (A1, A3, B), and these have been amply discussed in the literature. In anatase an additional feature (A2) is usually observed as a weak shoulder. There is general agreement in recent studies of the anatase Ti *K*-edge XANES that A3 and B are due to dipole-forbidden transitions of the core electron to *b1,e* (3d-4p) and *b2,a1* (3d-4p) hybridized states (see Luca et al.[61] and references therein). There is, however, less unanimity regarding assignment of the A1 and A2 transitions. However, Luca et al. showed that the intensity of these features are very dependent on particle size, and this led to their assignment to distorted surface sites. Such an interpreta-

(54) Sandroff, C. J.; Hwang, D. M.; Chung, W. M. *Phys. Rev. B* **1986**, *33*, 5953−5955.
(55) Sandroff, C. J.; Kelty, S. P.; Hwang, D. M. *J. Chem. Phys.* **1986**, *85*, 5337.
(56) Lamberti, C. *Microporous Mesoporous Mater.* **1999**, *30*, 155.
(57) Zhang, J.; Hu, Y.; Matsuoka, M.; Yamashita, H.; Minagawa, M.; Hidaka, H.; Anpo, M. *J. Phys. Chem. B* **2001**, *105*, 8395.
(58) Southon, P. D.; Howe, R. F. *Chem. Mater.* **2002**, *14*, 4209.
(59) Wang, Y.; Suna, A.; Mahler, W.; Kasowski, R. *J. Chem. Phys.* **1987**, *87*, 7315.
(60) Grunes, L. A. *Phys. Rev. B: Condens. Matter* **1983**, *27*, 2111.
(61) Luca, V.; Djajanti, S.; Howe, R. F. *J. Phys. Chem. B* **1998**, *102*, 10650.

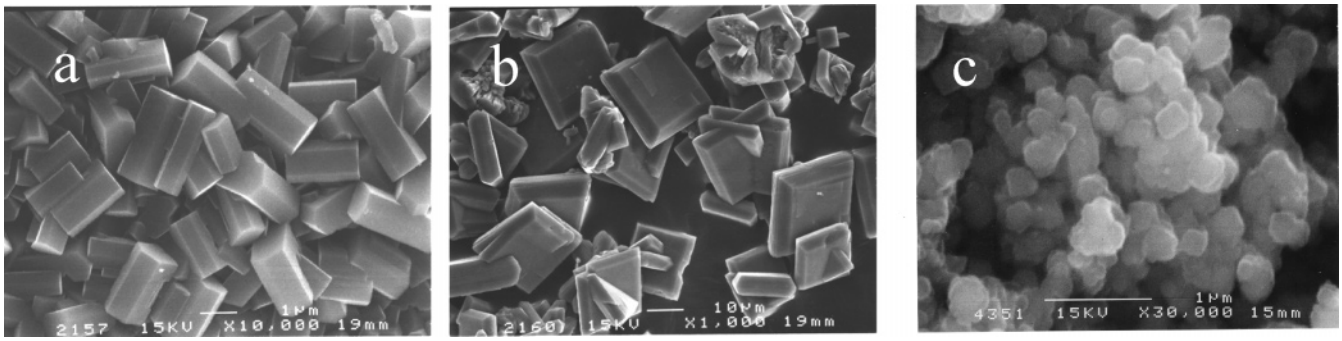

Figure 4. SEM images of (a) Nenadkevichite, (b) ETS-10, and (c) sitinakite.

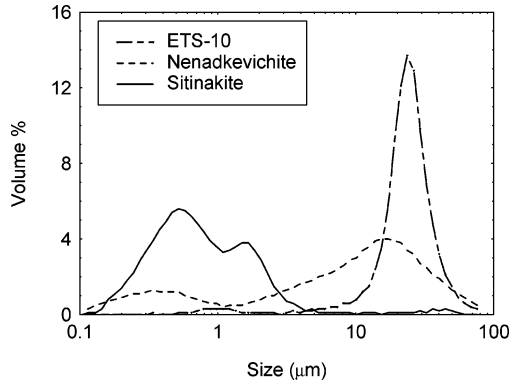

Figure 5. Particle size distributions for various titanosilicates.

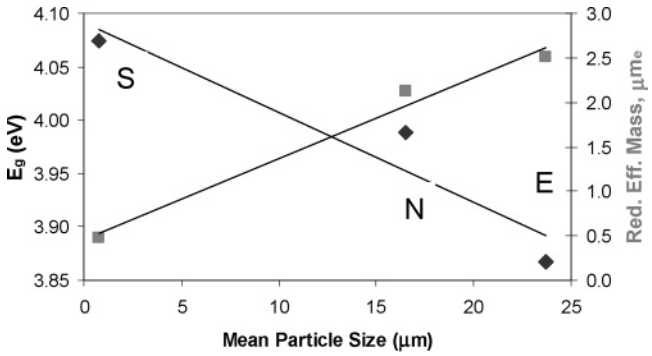

Figure 6. Variation of experimentally determined E_g (◆) and calculated reduced effective mass (■) with particles size for various titanosilicate quantum wires. S = sitinakite, N = nenadkevichite, E = ETS-10.

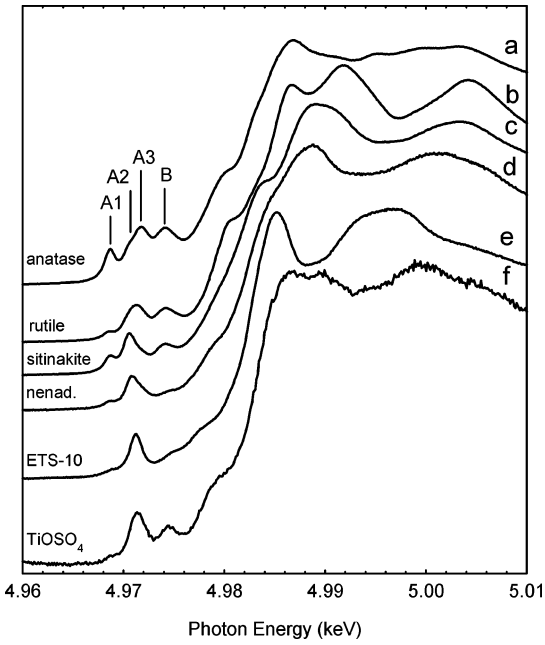

Figure 7. XANES spectra for various titanosilicates in comparison with standard TiO_2 materials: (a) nanocrystallinte anatase, (b) nanocrystalline rutile, (c) sitinakite, (d) nenadkevichite, (e) ETS-10, and (f) titanyl sulfate.

tion has generally been supported by others.[62,63] In contrast, the experimental pre-edge XANES structure of ETS-10 (Figure 7e) is characterized by a single relatively intense pre-edge feature at 4971.2 eV (Figure 7). In a similar fashion, this pre-edge feature in the spectrum of ETS-10 has recently been ascribed to distorted terminal Ti species in the titanate wires.[64] The general observation that can be made from the collection of pre-edge spectra in Figure 7 is that for the wire systems the central A2 and A3 transitions are well developed while A1 and B features are weak. This is especially true for the single-wire systems where A1 and B can barely be discerned and less so for the double wires in sitinakite (Figure 7c), the pre-edge structure of which strongly resembles that of rutile.

Such observations are therefore suggestive of colligative electronic properties being quickly manifest as the wire diameter increases despite the fact that there is an overall blue shift in gap energy due to the small crystallite size. It would be interesting to observe the effect on the XANES pre-edge as a function of sitinakite crystallite diameter were it possible to synthesize materials with different average crystallite dimensions.

Photocatalysis. The model photocatalytic reaction investigated in this study is the decomposition of methylene blue. Many studies of this photocatalytic reaction have been undertaken in recent times, and it has become something of a model system. MB has optical absorption in both the visible and UV regions (Figure 3) and displays a significant decay rate due to simple photolysis. Because of this, each photocatalytic run was preceded by a determination of the background rate which was subtracted from the data taken in the presence of a catalyst. This 'background' rate, while substantial, was determined to be steady and reproducible throughout our experiments, making comparisons between catalysts valid.

(62) Wu, Z. Y.; Zhang, J.; Ibrahim, K.; Xian, D. C.; Li, G.; Tao, Y.; Hu, T. D.; Bellucci, S.; Marcelli, A.; Zhang, Q. H.; Gao, L.; Chen, Z. Z. *Appl. Phys. Lett.* **2002**, *80*, 2973.
(63) Choi, H. C.; Ahn, H.-J.; Jung, Y. M.; Lee, M. K.; Shin, H. J.; Kim, S. B.; Sung, Y.-E. *Appl. Spectrosc.* **2004**, *58*, 598.
(64) Prestipino, C.; Solari, P. L.; Larnberti, C. *J. Phys. Chem. B* **2005**, *109*, 13132.

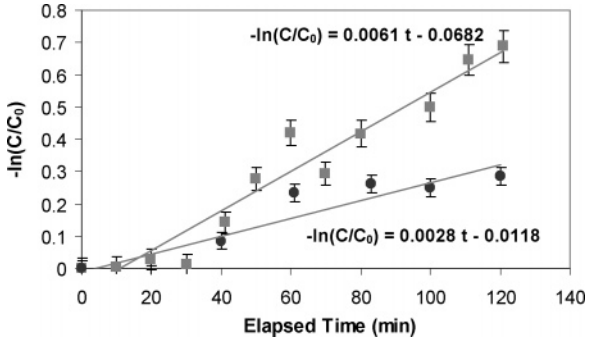

Figure 8. First-order kinetic plot comparing direct light photolysis in the absence (●) of catalyst and photocatalytic mineralization in the presence of catalyst P25 (■). In the latter case, a catalyst concentration of 0.522 g/L was used. Both experiments were performed at initial MB concentrations of 0.130 mM and pH 8.6. C_0 is the initial MB concentration, and C is the final MB concentration at a given elapsed time.

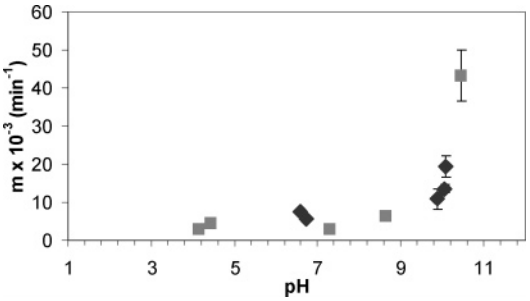

Figure 9. pH dependence of MB mineralization for sitinakite (◆) and P25 (■) using 0.522 g/L and 0.130 mM MB concentration. m is the pseudo-first-order rate constant.

Results of the degradation of MB in the presence and absence of catalyst under visible light are shown in Figure 8.

A linear dependence was observed between the ratio of mass of catalyst used to volume of solution, and this can be taken as further definitive evidence that the sitinakite functions in either a photocatalytic or photosensitization mode and not simple photolysis. The fact that the pH of the MB solution was found to decrease from its initial value during the course of the reaction is consistent with production of acid resulting from the mineralization of MB as previously described.[53,65]

At high solution pH values it is to be expected that the surfaces of suspended titanate catalysts should become increasingly negatively charged, thus favoring adsorption of the cationic MB. Clearly, the greater the amount of MB adsorbed onto the catalyst's surface, the easier it is for the dye to be degraded by reactive products formed at the catalyst's surface. The sitinakite sample tested had been prepared from a highly alkaline precursor gel, and even though it had been thoroughly washed with water, the suspension had a very high initial pH which could be reduced by addition of acid. Hence, it displayed substantial adsorption properties and also a high photocatalytic decay rate. Thus, reaction rate was extremely sensitive to the pH of the MB solution as demonstrated in Figure 9. Nevertheless, the pH values of most interest are around those observed in surface waters, i.e., around 7. Therefore, this study focuses in this region of pH.

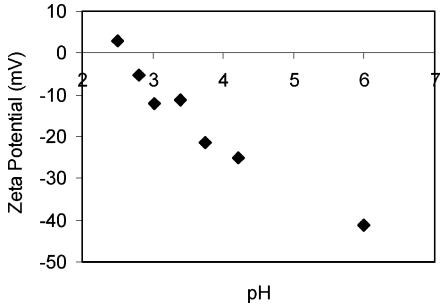

Figure 10. Zeta potential plot for sitinakite as a function of pH.

While the reaction rate is not insignificant at low pH values, it increases dramatically for initial solution pH values above 9. This can be attributed to the increased absorption of MB molecules on the catalyst surfaces at high pH values where the surface acquires a negative charge. For P25 the pH at the point of zero charge (pH_{pzc}) has been report to be between 6 and 6.6. In contrast, we measured the value of pH_{pzc} for the sitinakite to be 2.3 (Figure 10). Interestingly, this value is close to that of silica, which has $pH_{pzc} = 1.7-2.5$.[66] The low value of pH_{pzc} for sitinakite implies that the MB cation should sorb much more strongly on sitinakite than on P25 titania at the near neutral pH values which are relevant to water detoxification. In addition to measuring pH_{pzc} we directly measured MB adsorption isotherms for both sitinakite and P25 at pH 7. While in the case of sitinakite isotherms were of the Langmuir type, giving significant adsorption capacity (in the order of 0.122 mmol/g) at pH = 7, a very low capacity was observed for MB adsorption on P25 at this pH value. For a simple oxide such as TiO_2, it is clear from the value of pH_{pzc} that the surface charge will be very low. The surface charge of a simple, essentially stoichiometric oxide such as titania derives from termination of the lattice at the surfaces, resulting in surface charge that depends on solution pH. Although some surface charge can also be generated in this way, in a more complex microporous oxide material such as sitinakite the internal and external surfaces of sitinakite have a permanent negative charge that is due to a deficit of positive charge in the framework. This negative charge is compensated by exchangeable cations within the channels and also on the surfaces. At a pH of 10 the MB adsorption isotherm of sitinakite was also Langmuirian and the capacity that was obtained was even higher than at pH = 7. Again, P25 was observed to have a relatively low capacity relative to sitinakite.

A direct comparison of the photocatalytic activity of P25 and sitinakite measured under identical experimental and solution pH of 7 and after subtraction of the background rate is shown in Figure 11. As previously stated, this pH was chosen because it is the most relevant to surface water. It can be seen from the plot in Figure 11 that the activity of sitinakite is significantly higher than that of P25 ($m = 0.0076$, cf. $m = 0.0057$). At first this seems somewhat odd given that the band gap of sitinakite is extremely blue shifted compared with that of P25, suggesting that very little visible light energy is being absorbed by these catalysts. However,

(65) Houas, A.; Lachheb, H.; Ksibi, M.; Elaloui, E.; Guillard, C.; Herrmann, J. M. *Appl. Catal. B* **2001**, *31*, 145.

(66) Parks, C. A. *Chem. Rev.* **1965**, *15*, 177.

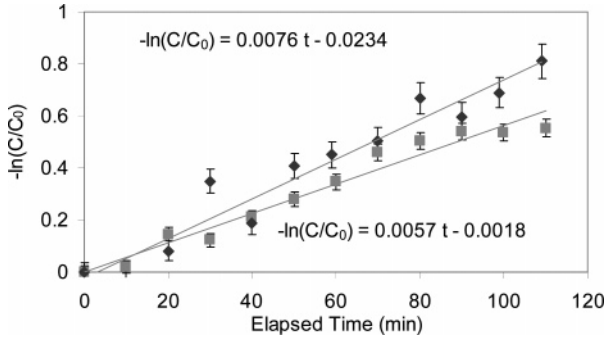

Figure 11. First-order kinetic plots comparing sitinakite (◆) and P25 (■) measured using visible light excitation. Experiments were performed at a catalyst concentration of 0.522 g/L, initial MB concentrations of 0.130 mM, and pH 6.7. C_0 is the initial MB concentration, and C is the final MB concentration.

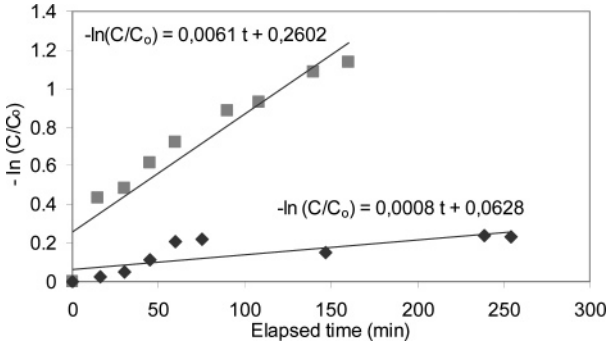

Figure 12. First-order kinetic plots for sitinakite (◆) and P25 (■) measured using UV excitation. Catalyst, MB concentration, and pH same as in Figure 11.

as previously mentioned, at pH 7 sitinakite adsorbs MB very strongly which itself can be photoexcited. Given that the sodium vapor lamp being used in this work gives very little emission below 400 nm and that the absorption edge of sitinakite is at very high energy, we expect negligible photoexcitation of electrons in the quantum wires using this excitation source. Therefore, it must be concluded that photodecomposition of MB using visible light excitation is occurring in the present system through efficient excitation of the dye and charge injection into the sitinakite conduction band. Obviously the conduction band edge has to be low enough in energy to facilitate this process. As the main purpose of this study is to provide an initial comparative evaluation of the capacity of sitinakite to bring about the photodecomposition of MB, it is beyond the scope of this work to determine these band positions exactly. Apart from matching dye excitation levels and semiconductor band structure, it is clear that chemisorption is playing a significant role in the present titanosilicate system.

Although the band gap of the as-prepared sitinakite in this study is very large, it is extremely interesting that it can function as a photocatalyst at all. It should be possible to change the nature of the band edge in this quantum-confined wide band gap semiconductor through cation doping in the framework and also by immobilizing other cations within the tunnel sites as demonstrated with incorporation of titanate species in zeolites. As a first attempt, we investigated the photocatalytic activity of sitinakite materials containing a range of exchangeable cations including Ag^+, Co^{2+}, Cu^{2+}, and Fe^{3+}. All of these cation variants performed more poorly than the parent or Na^+-exchanged material. This suggests that extra framework cation acidity is not relevant to MB photodegradation. We are presently investigating the performance of sitinakite materials in which heteroatoms are substituted for Ti in framework sites.

Given the position of the sitinakite band gap compared to P25, we further investigated the photodegradation of MB using UV excitation and similar conditions used during the visible light excitation measurements (Figure 12). The data of Figure 12 show that, as might be expected, the rate of photodegradation under these conditions is much greater for P25 than for sitinakite. However, the degradation rate using sitinakite was still significantly above the background rate. With the narrow black light emission centered at 360 nm (Figure 1b) it is clear that while P25 with an absorption onset at about 400 nm can be excited by this light source, sitinakite, with absorption onset at about 340 nm, will not. Thus, photodegradation in the UV regions must also derive from excitation or sensitization of the dye.

Conclusions

In this study the optical and electronic properties of titanosilicate materials have been compared with those of nanocrystalline rutile and anatase. Sitinakite, like ETS-10, is a very wide band gap semiconductor due to the quantum wires that form part of its structure. The band edge of sitinakite is somewhat more blue shifted than that of ETS-10 even though the wire diameter of sitinakite is twice that of ETS-10. In the framework of the EMM this can be explained as being due to the reduced effective mass of electrons and holes in sitinakite being much smaller than it is for ETS-10. Although the wide band gap of sitinakite should make this material a poorer visible light photocatalyst than 'standard' titania materials, it has in fact been found to display superior performance for MB photodegradation. The improved activity of sitinakite appears to be due to the stronger propensity for adsorption displayed by this material for the cationic MB dye and the fact that degradation is due to photosensitization of the dye leading to charge injection into the quantum wire semiconductor.

Acknowledgment. X-ray absorption experiments were supported by the Australian Research Council. Access to the Photon Factory was provided by the Australian Synchrotron Research Program which has been funded by the Commonwealth of Australia via the Major National Research Facilities Program. We are particularly indebted to Dr. Garry Foran for assistance with the X-ray absorption measurements and determination of the instrumental resolution. The authors are also grateful to colleagues E. Drabarek and D. Cassidy of ANSTO for assistance with construction of the reactor used for visible light irradiations.

Supporting Information Available: X-ray powder diffraction patterns. This material is available free of charge via the Internet at http://pubs.acs.org.

CM052839P